


**Jahn-Teller effect in three-body recombination of hydrogen atoms**Chi Hong Yuen  and Viatcheslav Kokoouline*Department of Physics, University of Central Florida, Orlando, Florida 32816, USA* (Received 5 December 2019; revised manuscript received 7 February 2020; accepted 23 March 2020; published 28 April 2020)

The three-body recombination rate coefficients of the  $\text{H} + \text{H} + \text{H} \rightarrow \text{H}_2 + \text{H}$  process for different final rovibrational levels of  $\text{H}_2$  are determined using a fully quantum-mechanical approach at zero total angular momentum. The Jahn-Teller coupling between the lowest electronic states of the  $\text{H}_3$  system is accounted for. It is found that the Jahn-Teller effect substantially enhances the recombination rates for deeply bound dimers at room temperature but only leads to a 12% increase in the total three-body recombination rate. It is also found that the nascent population of the  $\text{H}_2$  molecules, formed in the recombination process, is dominated by highly excited rovibrational levels.

DOI: [10.1103/PhysRevA.101.042709](https://doi.org/10.1103/PhysRevA.101.042709)**I. INTRODUCTION**

The three-body recombination (TBR) of hydrogen atoms,  $\text{H} + \text{H} + \text{H} \rightarrow \text{H}_2 + \text{H}$ , plays a key role in the formation of the first generation of stars in the Universe. This process is the main mechanism in the interstellar medium (ISM) for the conversion of atomic hydrogen to the molecular form in a gas phase at large densities  $n_H$  of the atomic hydrogen [1]. Since this reaction is highly exothermic, the energy released during the process contributes to the heating of the primordial gas. At the same time, due to its large abundance compared to other species in the ISM,  $\text{H}_2$  molecules produced from this reaction cool down radiatively the primordial gas at  $n_H > 10^8 \text{ cm}^{-3}$  [2]. Therefore, TBR of  $\text{H}_3$  strongly influences the thermal and dynamical evolution of the gas [3–6]. However, at relevant temperatures,  $200 \text{ K} < T < 2000 \text{ K}$ , rate coefficients for the TBR of  $\text{H}_3$  reported in different studies disagree with each other by two orders of magnitude [1, 7–9]. Such an uncertainty in the magnitude of the rate coefficient leads to a significant uncertainty in models of the evolution of the primordial gas [4–6].

The TBR of  $\text{H}_3$  is also a problem of a fundamental interest in atomic and molecular physics. With the three lightest indistinguishable nuclei, the  $\text{H}_3$  system is described by the  $S_3 \otimes I$  complete nuclear permutation and inversion group ( $S_3$  is the group of permutations of three identical particles, and  $I$  is the inversion operator), or considering a dynamical picture of vibration or scattering, by the point-group  $D_{3h}$  isomorphic to  $S_3 \otimes I$ . The ground electronic state is the doubly degenerate state of the  $E'$  irreducible representation (irrep) of  $D_{3h}$  at the equilateral geometry of  $\text{H}_3$  and splits into two electronic states near that geometry, producing a conical intersection between the two lowest potential-energy surfaces (PESs) of  $\text{H}_3$  [10, 11]. Consequently, the nonadiabatic coupling between the two states diverges at the conical intersection such that the Born-Oppenheimer approximation breaks down and the nuclei motion is strongly coupled to the electronic motion [12]. This coupling, which arises from the symmetry of the system, is also known as the Jahn-Teller coupling [13]. Cer-

tain effects of the Jahn-Teller coupling could be represented using the lowest potential-energy surface only by introducing the geometric phase. In the reactive scattering of  $\text{H} + \text{HD}$  [14], the effect of the geometric phase was studied. However, the complete Jahn-Teller physics involving two PESs has not so far been studied in the TBR process.

Although fully quantum-mechanical approaches for the TBR on a single PES have been developed [15, 16], the systems studied were often at ultracold temperatures with model potentials [16–19] or only supported a few bound states on a realistic PES [20]. To date, TBR cross sections for realistic systems which support a large number of bound states at an intermediate-energy range have not been reported. One of the obstacles is to represent a considerable amount of sharp avoided crossings between numerous adiabatic channels. Hyperspherical adiabatic (HSA) approaches which utilized the slow variable discretization [21] were developed to represent such nonadiabatic couplings [18, 22, 23] and were proven to be robust computationally. Such approaches could resolve the complication in the case of  $\text{H}_3$  where more than 150 adiabatic channels are involved. In addition, despite the fact that the Jahn-Teller couplings were introduced into the HSA approach for the calculation of predissociative states of  $\text{H}_3$  [24], it has not yet been implemented into the HSA approach with the eigenchannel  $R$ -matrix (HSAR) method [23, 25] for TBR problems.

Due to technical difficulties of a fully quantum-mechanical approach, rate coefficients for the TBR of  $\text{H}_3$  in previous studies were obtained using various assumptions and approximations. Orel [26] has computed the TBR rate coefficient ( $1.3 \times 10^{-32} \text{ cm}^6/\text{s}$  at 300 K) using a combination of the orbiting resonance theory [27] and the quasiclassical trajectory method. Based on the principle of detailed balance, Palla *et al.* [1] and Flower and Harris [7] used the rate coefficient for collision-induced dissociation  $\text{H}_2 + \text{H} \rightarrow \text{H} + \text{H} + \text{H}$  measured in the experiment [28] to evaluate the TBR rate coefficient ( $1.8 \times 10^{-31}$  [1] and  $2.2 \times 10^{-30} \text{ cm}^6/\text{s}$  [7] at 300 K). Blandon and Kokoouline [24] obtained an estimate ( $\sim 2 \times 10^{-30} \text{ cm}^6/\text{s}$

at 300 K) for the coefficient from positions and widths of predissociated  $H_3$  resonances produced by two lowest electronic states of  $H_3$  coupled by the Jahn-Teller coupling. Esposito and Capitelli [29] have evaluated the coefficient using the quasiclassical trajectory method, similar to Orel [26]. A more recent study by Forrey [9,30] has made an important step towards a fully quantum approach where continuum states of  $H_2$  were included and quantum-mechanical formalism for the three-body dynamics was used, and obtained the value of  $2.6 \times 10^{-32} \text{ cm}^6/\text{s}$  at 300 K. Unfortunately, there is no clear criteria to determine which value of the rate coefficient is the most accurate because there are no experimental data for the TBR process or a fully quantum-mechanical and reliable theoretical benchmark study for a comparison.

In the present paper, we employ the HSAR method to compute the continuum functions of the  $H_3$  system, the TBR cross section, and rate coefficient at zero total angular momentum  $J$ . The interaction potential of the system includes the two lowest electronic states of  $H_3$  coupled by the Jahn-Teller coupling, similar to the previous study [24]. We compare results obtained with and without the Jahn-Teller couplings and find that the Jahn-Teller coupling enhances the total recombination rate by about 12% at  $T = 300 \text{ K}$ . Our results suggest that the Jahn-Teller effect is not that important for the total TBR rate coefficient of  $H_3$  at  $J = 0$ , but the effect could be observed by measuring branching ratios with respect to final rovibrational levels of the formed  $H_2$  molecule. A similar measurement has been recently made in the experiment on the  $Rb_3$  recombination [19].

## II. THEORETICAL APPROACH

To compute the total TBR rate coefficient, we used the method described in Ref. [23] and references therein. In the method, the HSA eigenvalue equation is solved for several fixed values of the hyper-radius  $\rho$ ,

$$\left[ \hbar^2 \frac{\Lambda^2 + \frac{15}{4}}{2\mu\rho^2} + V(\rho, \theta, \phi) \right] \varphi_a(\rho; \theta, \phi) = U_a(\rho) \varphi_a(\rho; \theta, \phi), \quad (1)$$

where  $(\theta, \phi)$  are the hyperangles,  $\mu$  is the three-body reduced mass,  $\Lambda^2$  is the grand angular momentum operator at  $J = 0$  [31], and  $V$  is the interaction potential. Next, the HSA channel functions are used to construct the total nuclear wave function. The hyper-radial Schrödinger equation is solved using the eigenchannel  $R$ -matrix method [25]. The solution gives continuum three-body wave functions and the scattering  $S$ -matrix. Then, the thermally averaged rate coefficient at  $J = 0$  is obtained as [23]

$$\langle K_3 \rangle(T) = \frac{1}{2(k_b T)^3} \int K_3(E) e^{-E/k_b T} E^2 dE, \quad (2)$$

$$K_3(E) = \frac{32\hbar\pi^2}{\mu k^4} \sum_{f,i} |S_{f \leftarrow i}|^2,$$

where  $k$  is the initial wave number and  $i$  and  $f$  refer to three-body and dimer-atom channels, respectively. Note that the prefactor at the TBR rate coefficient  $K_3$  is six times smaller than in Ref. [20] due to a different convention. In

our convention, the three-body loss rate is obtained by  $L_3 = 3\langle K_3 \rangle$ , which is equivalent to Ref. [20].

To account for the Jahn-Teller coupling between the  $1^2A'$  and the  $2^2A'$  electronic states of  $H_3$ , we adopt the diabaticization procedure of Ref. [24]. A similar approach was also used in Ref. [32].

In the diabatic basis of two electronic states of  $H_3$ , two degenerate electronic states were chosen to be the  $|E'_+\rangle$  and  $|E'_-\rangle$  states of the  $E'$  irrep of the  $D_{3h}$  symmetry group. The diabatic vibronic wave function in this basis is represented as

$$\Psi = \psi_+ |E'_+\rangle + \psi_- |E'_-\rangle. \quad (3)$$

The interaction potential  $V$  becomes a  $2 \times 2$  diabatic potential and is approximated as

$$V = \frac{1}{2} \begin{pmatrix} V_1 + V_2 & (V_1 - V_2)e^{i\phi} \\ (V_1 - V_2)e^{-i\phi} & V_1 + V_2 \end{pmatrix}, \quad (4)$$

where  $V_1$  and  $V_2$  are the  $1^2A'$  and  $2^2A'$  PESs of  $H_3$  from Ref. [10] and  $\phi$  is the angle of the diabatic transformation [24,32]. In this approach, the couplings due to first derivatives of the  $1^2A'$  and  $2^2A'$  PESs are neglected. This approximation is justified by a good agreement for energies and widths of predissociated levels of  $H_3$  obtained in Ref. [24] where the couplings were neglected with the results of Ref. [33] where the couplings were accounted for. Although this diabatic potential was derived near the conical intersection, we will use it globally in this approximation. Detailed discussion on the choice of rotation angle for the diabatic transformation can be found in Ref. [32] and references therein.

Since the three nuclei of  $H_3$  are identical fermions, the total wave function should transform in the  $D_{3h}$  group as the  $A'_2$  or  $A''_2$  irreps. For  $J = 0$ , the rotational wave function is totally symmetric in the group. As a result, the irrep of the total wave function is determined by a direct product of irreps of vibronic and nuclear-spin wave functions. The two lowest electronic states, taken into account in this paper, transform in the group as two components of the  $2E'$  irrep. The electronic spin is  $1/2$ , thus, the electronic spin function is of the  $E$  irrep also (in the electron-permutation group). Since each nucleus has spin  $1/2$ , the total nuclear-spin wave function can be of the  $A_1$  or  $E$  irreps of the  $S_3$  symmetry group (a subgroup of  $D_{3h}$ ). Because  $E \otimes E = A_1 \oplus A_2 \oplus E$ , for the total wave function to be of the  $A'_2$  or  $A''_2$  irreps, the vibrational part  $\psi_{\pm}$  of the total wave function can transform as the  $A_1$ ,  $A_2$ , or  $E$  irreps in its  $S_3$  symmetry group. In this paper, we consider vibrational wave functions of the  $A_1$  irrep only.

## III. COMPUTATIONAL DETAILS

In the HSAR approach, the hyperangular wave functions  $\varphi_a(\rho; \theta, \phi)$  are expanded in terms of  $B$ -spline functions  $u$  and  $v$ ,

$$\varphi_a(\rho; \theta, \phi) = \sum_{ij} b_{ij,a}(\rho) u_i(\theta) v_j(\phi),$$

where the interval of  $\theta$  and  $\phi$  are  $[0, \pi/2]$  [34] and  $[-\pi/2, -\pi/6]$  [35], respectively. At large hyper-radii, the hyperangular wave functions for dimer-atom channels are highly localized at  $\theta = \pi/2$  and  $\phi = -\pi/2$ . To better represent

dimer-atom channels, we used the following hyperangular grids with variable grid steps:

$$\theta_i = \frac{\pi}{2} [1 - (1 - t_i)^7], \quad t_i = \frac{i-1}{N_\theta - 1},$$

$$\phi_j = \frac{\pi}{3} \tanh \frac{t_j - 1}{L} - \frac{\pi}{6}, \quad t_j = \frac{j-1}{N_\phi - 1},$$

where  $N_\theta$  and  $N_\phi$  are the number of grid points for  $\theta$  and  $\phi$  and  $L$  is a parameter for tuning the distribution of the grid points. In the present paper, we chose  $N_\theta = N_\phi = 140$  and  $L = 0.2$  such that the hyperangular grids are sufficiently dense in the region near  $\theta = \pi/2$  and  $\phi = -\pi/2$ .

For the hyper-radius grid, we adopt the variable grid described in Refs. [22,35], where  $\rho$  varies from 1.5 to  $46a_0$  with 512 steps. To represent numerous sharp avoided crossings between adiabatic potentials, we expanded the continuum hyper-radial wave function in terms of  $B$ -spline functions  $\pi_j(\rho)$  such that the nuclear wave function  $\Phi$  becomes

$$\Phi(\rho, \theta, \phi) = \sum_{j,a} c_{j,a} \pi_j(\rho) \varphi_a(\rho; \theta, \phi).$$

The hyper-radial Schrödinger equation then becomes

$$\sum_{j,a} \left[ \langle \pi_{j'} | \left( -\frac{\hbar^2}{2\mu} \frac{d^2}{d\rho^2} \right) | \pi_j \rangle O_{j'a',ja} + \delta_{aa'} \langle \pi_{j'} | U_a(\rho) | \pi_j \rangle - E \langle \pi_{j'} | \pi_j \rangle \delta_{aa'} \right] c_{j,a} = 0, \quad (5)$$

where  $O_{j'a',ja} = \langle \varphi_{a'}(\rho_{j'}; \theta, \phi) | \varphi_a(\rho_j; \theta, \phi) \rangle$  and is integrated over hyperangles only. Note that, although the above equation is different from the one in Refs. [23,35], it has the same numerical accuracy.

On the other hand, since the Hamiltonian is complex, the hyperangular wave functions  $\varphi_a(\rho; \theta, \phi)$  obtained by solving Eq. (1) contain nontrivial phase factors. As a result,  $O_{j'a',ja}$  and the  $R$  matrix will be complex. To obtain a real  $R$  matrix, a phase convention is, therefore, needed for  $\varphi_a(\rho; \theta, \phi)$  [25]. We fixed the phase in a way similar to Ref. [20], but, instead, we chose the reference wave function to be the hyperangular wave function of a particular channel at the last step of the hyper-radius. Inspection of the elements  $O_{j'a',ja}$  indicated that all elements became real after this procedure.

#### IV. RESULTS AND DISCUSSION

Figure 1 displays HSA potential-energy curves  $U_a$  at  $J = 0$ . Some 200 HSA channels are included in the  $R$ -matrix calculation. Channels that converge to the  $H + H + H$  dissociation limit of ( $E = 0$ ) are three-body channels, which are shown in the inset of Fig. 1. Since the  $2^2A'$  PES is repulsive, the 156 allowed dimer-atom channels, which converge to the dissociation limit of  $H_2(\nu, j) + H$  are all from the  $1^2A'$  PES. The Jahn-Teller coupling mixes the three-body channels from the two PESs. To demonstrate contributions from each PES, we have obtained HSA curves using only the lowest adiabatic  $1^2A'$  PES. Figure 2 shows a zoomed region of Fig. 1 near the  $H + H + H$  dissociation limit. The dashed lines are the HSA curves obtained using only the  $1^2A'$  PES. The three-body channels from the  $2^2A'$  PES are the curves that do not overlap

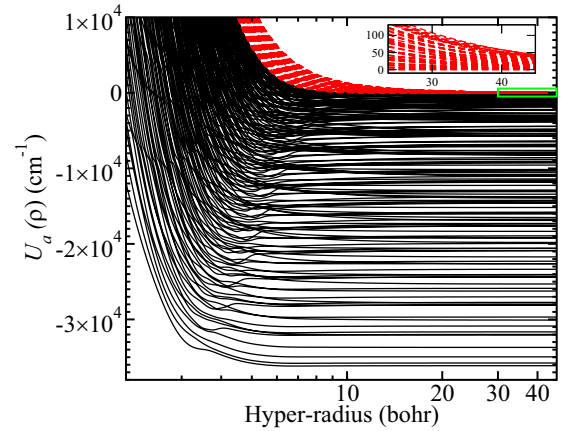


FIG. 1. HSA potential-energy curves for  $H_3$ . The x-axis is in log-scale. Channels that converge to the  $H + H + H$  dissociation limit at the energy  $E = 0$  are three-body channels (dashed lines). The other curves converging to different  $H_2(\nu, j) + H$  thresholds are the dimer-atom channels (solid lines). The inset zooms at the region of large hyper-radii near the  $H + H + H$  dissociation limit.

with the dashed lines. Note that the lowest three-body HSA curve of the  $2^2A'$  PES (indicated by the smaller arrow in Fig. 2) has a barrier. It means that the probability of the  $H + H + H \rightarrow H_2 + H$  transition from that channel is small at low energies and that the Jahn-Teller effect on the TBR of  $H_3$  at low temperatures is expected to be small. For higher total angular momenta, since the potential barrier will be higher, in general, one expects the Jahn-Teller effect will be weaker compared to the case of  $J = 0$  at a fixed collision energy.

Figure 3 shows the thermally averaged rate coefficient  $\langle K_3 \rangle$  obtained using Eq. (2). To assess the importance of the Jahn-Teller effect, we also computed  $\langle K_3 \rangle$  using the single  $1^2A'$  PES. The solid and dashed lines represent the total TBR rate coefficients obtained in the two-PES model [Eq. (4)] and the single PES model. The inset of Fig. 3 shows the percentage difference between the rate coefficients calculated in the two models. One can see that the Jahn-Teller effect in

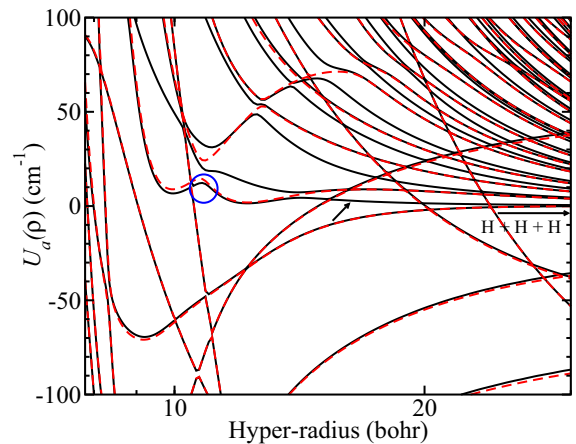


FIG. 2. A zoom of Fig. 1. The x-axis is in log-scale. The dashed lines are the HSA energy curves obtained using only the  $1^2A'$  PES, whereas the solid lines are the curves obtained using the complete potential of Eq. (4).

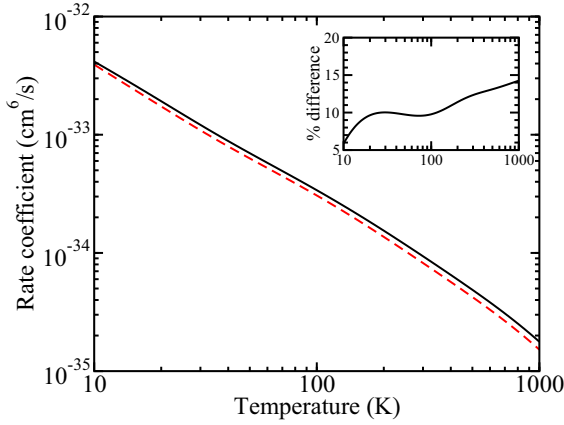


FIG. 3. Thermally averaged total TBR rate coefficients as a function of temperature, obtained using the full potential of Eq. (4) (solid line) and the single uncoupled  $1^2A'$  PES (dashed line). The inset shows the percentage difference  $(K_{\text{two PESs}} - K_{\text{one PES}})/K_{\text{two PESs}} \times 100$ .

the total TBR rate is stronger at higher temperatures, but the enhancement is less than 15% in the interval of 10–1000 K. The strong temperature dependence at  $T = 10$ –20 K can be explained by the above-mentioned energy barrier for the  $H + H + H \rightarrow H_2 + H$  transition as the barrier has a height of about  $12 \text{ cm}^{-1}$  (17 K). This also seems to support our conjecture on the Jahn-Teller effect at higher total angular momenta. Overall, since the uncertainty of the rate coefficient due to the numerical convergence of the present calculation (mainly due to different hyperangular grids) is about 10%, we conclude that the Jahn-Teller coupling has a small effect on the total TBR rate at  $J = 0$  for temperatures of  $T = 10$ –1000 K.

In Fig. 3, one may note that our total TBR rate coefficient at 300 K ( $\sim 1 \times 10^{-34} \text{ cm}^{-6}/\text{s}$ ) is a few orders of magnitude smaller than rate coefficients obtained in the previous studies. It is because we consider a very limited case where  $J = 0$  and vibrational wave functions transform as the  $A_1$  irrep. To have a meaningful comparison with the results from the previous studies, one must include contributions due to different  $J$ 's and other irreps of the vibrational wave functions. However, such cases are still challenging to be solved within the HSAR approach and are beyond the scope of this paper.

It is instructive to see thermally averaged TBR rate coefficients  $\langle K_{3,f} \rangle$  into a particular final two-body channel  $f$ ,

$$\langle K_{3,f} \rangle(T) = \frac{1}{2(k_b T)^3} \int K_{3,f}(E) e^{-E/k_b T} E^2 dE,$$

$$K_{3,f}(E) = \frac{32\hbar\pi^2}{\mu k^4} \sum_i |S_{f \leftarrow i}|^2.$$

Figure 4 shows the  $\langle K_{3,f} \rangle$  coefficients at  $T = 300 \text{ K}$  as a function of binding energy  $E_b$  of the final products  $f$ . Circles and squares in the figure are the results obtained from the coupled two-PES potential [Eq. (4)] and the single  $1^2A'$  PES, respectively. For both models, the nascent distribution of the  $H_2$  molecules is dominated by highly excited rovibrational levels. At  $E_b < 10^4 \text{ cm}^{-1}$ , the values of  $\langle K_{3,f} \rangle$  obtained in the two models are similar. At larger binding energies, the coefficients obtained in the two-PES model with the Jahn-Teller

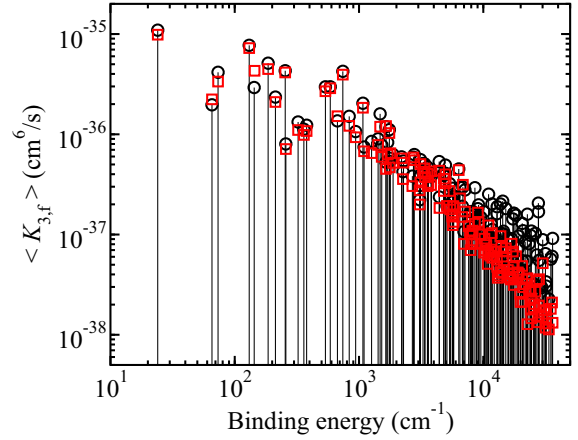


FIG. 4. Rate coefficients  $\langle K_{3,f} \rangle$  for recombination into a particular final dimer-atom channel  $f$  as a function of binding energy of the channel at 300 K. Circles correspond to the calculation with the complete two PESs of Eq. (4), and squares correspond to the calculation with a single  $1^2A'$  adiabatic PES.

coupling, are, in general, larger, up to ten times larger for some deeply bound dimers. Therefore, the 12% enhancement in the total TBR rate at 300 K from the Jahn-Teller effect is due to the substantial increase in the recombination rate towards deeply bound dimers. Indeed, we found that nonadiabatic couplings between the deeply bound dimer-atom channels and the three-body channels are larger for the two-PES model than the single PES model. On the other hand, for  $E_b > 10^4 \text{ cm}^{-1}$ , we found that the  $\langle K_{3,f} \rangle$  coefficients obtained in the single PES model scale as  $1/E_b^{1.5}$ , whereas it was difficult to find a scaling law for the coefficients obtained from the two-PES model due to their oscillatory behavior. The results suggest that the effect of the Jahn-Teller coupling in the TBR of  $H_3$  could be observed experimentally by measuring branching ratios of reaction products and looking at the dependence of the ratios as a function of binding energies, similarly as was performed in Ref. [19].

## V. CONCLUSION

In the present paper, we have determined thermal rate coefficients for TBR of the  $H + H + H \rightarrow H_2 + H$  reaction as a function of binding energies of  $H_2$  products for the total angular momentum  $J = 0$  using a fully quantum-mechanical approach. The role of the Jahn-Teller coupling in TBR is investigated for the case of the simplest neutral triatomic system  $H_3$  at zero total angular momentum. In this paper, we found that the effect of the Jahn-Teller coupling is small at low temperatures, whereas above 300 K, the effect enhances recombination rates significantly for the majority of deeply bound dimers but contributes only about 12% to the increase in the total TBR rate coefficient. Our results also suggest that the Jahn-Teller effect in TBR of  $H_3$  should be weaker at higher total angular momenta.

In addition, the rate coefficients obtained for individual final channels show that, in the recombination process, highly excited rovibrationally  $H_2$  molecules are formed preferentially. Considering the environment of interstellar clouds, the

excited molecules have different reactivity in collisions with other species compared to the ground-state  $H_2$  [36]. Therefore, the conclusion of the paper about the nascent distribution of mainly excited  $H_2$  could be very important for astrophysical models of thermal and chemical evolutions of interstellar clouds with a significant fraction of atomic hydrogen.

Our results represent significant progress in a fully quantum-mechanical study of the fundamental process of  $H_3$  TBR. The paper could also be considered a benchmark treatment: In the future, the accuracy of alternative approximate theoretical approaches for the TBR, such as the quasi-

classical trajectory approach [37], could be tested. Eventually, with a computationally feasible approach, once it is tested for  $J = 0$  and compared with the present results, an accurate and complete TBR rate coefficient could be obtained.

#### ACKNOWLEDGMENT

This work was supported by the National Science Foundation Grant No. PHY-1806915. The authors acknowledge the Advanced Research Computing Center at University of Central Florida for the high performance computing resources.

- 
- [1] F. Palla, E. Salpeter, and S. W. Stahler, *Astrophys. J.* **271**, 632 (1983).
- [2] S. Glover and D. W. Savin, *Mon. Not. R. Astron. Soc.* **393**, 911 (2009).
- [3] S. Glover, *AIP Conf. Proc.* **990**, 25 (2008).
- [4] M. J. Turk, P. Clark, S. C. Glover, T. H. Greif, T. Abel, R. Klessen, and V. Bromm, *Astrophys. J.* **726**, 55 (2010).
- [5] S. Bovino, D. Schleicher, and T. Grassi, *Astron. Astrophys.* **561**, A13 (2014).
- [6] J. Dutta, B. B. Nath, P. C. Clark, and R. S. Klessen, *Mon. Not. R. Astron. Soc.* **450**, 202 (2015).
- [7] D. Flower and G. Harris, *Mon. Not. R. Astron. Soc.* **377**, 705 (2007).
- [8] T. Abel, G. L. Bryan, and M. L. Norman, *Science* **295**, 93 (2002).
- [9] R. C. Forrey, *Astrophys. J. Lett.* **773**, L25 (2013).
- [10] A. Varandas, F. Brown, C. Mead, D. Truhlar, and N. Blais, *J. Chem. Phys.* **86**, 6258 (1987).
- [11] R. Abrol and A. Kuppermann, *J. Chem. Phys.* **116**, 1035 (2002).
- [12] D. R. Yarkony, *Rev. Mod. Phys.* **68**, 985 (1996).
- [13] H. A. Jahn and E. Teller, *Proc. R. Soc. London A* **161**, 220 (1937).
- [14] D. Yuan, Y. Guan, W. Chen, H. Zhao, S. Yu, C. Luo, Y. Tan, T. Xie, X. Wang, Z. Sun, D. H. Zhang, and X. Yang, *Science* **362**, 1289 (2018).
- [15] P. O. Fedichev, M. W. Reynolds, and G. V. Shlyapnikov, *Phys. Rev. Lett.* **77**, 2921 (1996).
- [16] B. D. Esry, C. H. Greene, and J. P. Burke, *Phys. Rev. Lett.* **83**, 1751 (1999).
- [17] H. Suno, B. D. Esry, and C. H. Greene, *Phys. Rev. Lett.* **90**, 053202 (2003).
- [18] J. Wang, J. P. D’Incao, and C. H. Greene, *Phys. Rev. A* **84**, 052721 (2011).
- [19] J. Wolf, M. Deiß, A. Krütkow, E. Tiemann, B. P. Ruzic, Y. Wang, J. P. D’Incao, P. S. Julienne, and J. H. Denschlag, *Science* **358**, 921 (2017).
- [20] H. Suno, B. D. Esry, C. H. Greene, and J. P. Burke, Jr, *Phys. Rev. A* **65**, 042725 (2002).
- [21] O. I. Tolstikhin, S. Watanabe, and M. Matsuzawa, *J. Phys. B: At., Mol. Opt. Phys.* **29**, L389 (1996).
- [22] V. Kokoouline and F. Masnou-Seeuws, *Phys. Rev. A* **73**, 012702 (2006).
- [23] C. H. Yuen and V. Kokoouline, *Eur. Phys. J. D* **71**, 19 (2017).
- [24] J. Blandon and V. Kokoouline, *Phys. Rev. Lett.* **102**, 143002 (2009).
- [25] M. Aymar, C. H. Greene, and E. Luc-Koenig, *Rev. Mod. Phys.* **68**, 1015 (1996).
- [26] A. Orel, *J. Chem. Phys.* **87**, 314 (1987).
- [27] R. E. Roberts, R. Bernstein, and C. Curtiss, *J. Chem. Phys.* **50**, 5163 (1969).
- [28] T. Jacobs, R. Giedt, and N. Cohen, *J. Chem. Phys.* **47**, 54 (1967).
- [29] F. Esposito and M. Capitelli, *J. Phys. Chem. A* **113**, 15307 (2009).
- [30] R. C. Forrey, *Phys. Rev. A* **88**, 052709 (2013).
- [31] B. Johnson, *J. Chem. Phys.* **79**, 1916 (1983).
- [32] B. K. Kendrick, *J. Chem. Phys.* **148**, 044116 (2018).
- [33] B. Lepetit, R. Abrol, and A. Kuppermann, *Phys. Rev. A* **76**, 040702(R) (2007).
- [34] B. Johnson, *J. Chem. Phys.* **73**, 5051 (1980).
- [35] J. Blandon, V. Kokoouline, and F. Masnou-Seeuws, *Phys. Rev. A* **75**, 042508 (2007).
- [36] I. Simbotin and R. Côté, *New J. Phys.* **17**, 065003 (2015).
- [37] J. Pérez-Ríos, S. Ragole, J. Wang, and C. H. Greene, *J. Chem. Phys.* **140**, 044307 (2014).